A Model for the Dispersion of Two-Phase Multicomponent Jets

G. A. Melhem and R. Saini

Prepared for Presentation at:

1992 Process Plant Safety Symposium

Houston, Texas

Arthur D. Little, Inc.

February, 1992

Unpublished

A Model for the Dispersion of Two-phase Multicomponent Jets

G. A. Melhem and R. Saini
Modeling & Simulation Unit
Arthur D. Little, Inc., Cambridge, Massachusetts

Summary

This paper develops a new model for the dispersion of two-phase flashing jets for multicomponent mixtures. The model is based on a numerical solution of the conservation equations for mass, momentum, energy and phase/chemical equilibrium. The model accounts for elevation, angle of release, jet-expansion, and the non-ideal behavior of water-aerosol mixtures. In addition, a new method for estimating liquid aerosol rainout is developed using droplet evaporation and a mean droplet size estimation technique based on available energy concepts. Droplet evaporation is shown to be an important factor in calculating liquid aerosol rainout. Model predictions are shown to be in good agreement with reported experimental data in both the near and far fields.

Model Structure

Figure 1 shows a general schematic of the model. The model is divided into four major components:

- source term characterization,
- aerosol formation,
- droplet evaporation, and
- jet conservation laws.

In source term characterization the source geometry, release type, and initial conditions are established. Source geometries include leakage through cracks

and openings, emergency relief, and pipe ruptures. Release types include gas/vapor, subcooled liquid, saturated flashing liquid and two-phase flow. Initial conditions established include release mass flow rate, temperature, flash fraction, expanded diameter, etc.

Figure 1: Model structure

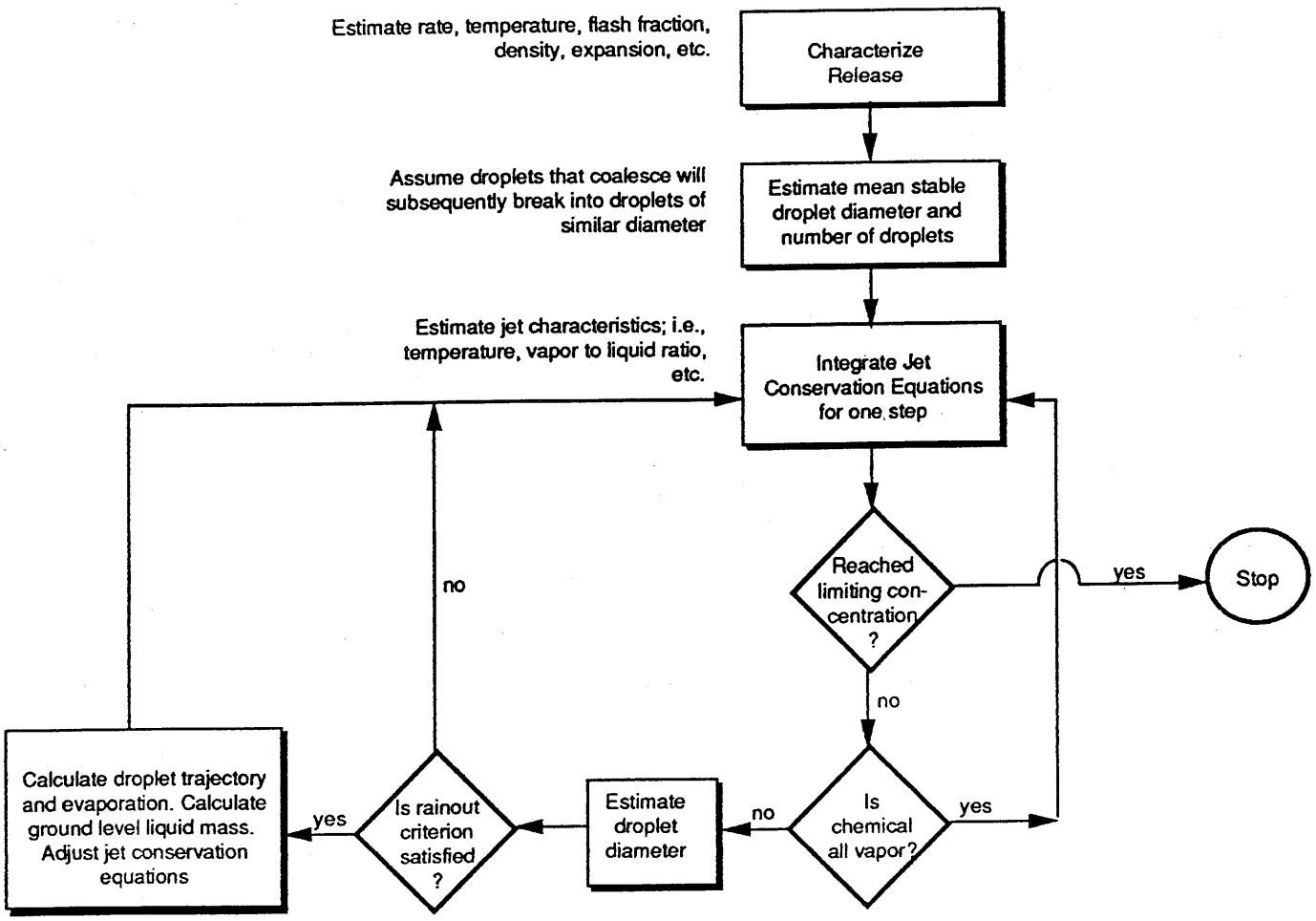

Aerosol Formation

The formation of liquid aerosols following loss of containment is an important aspect of source term characterization for both pressurized and non-pressurized liquid releases. The entrainment of liquid droplets in a vapor cloud increases the cloud density and subsequently alters its dispersion behavior. When dispersed, heavier than air clouds cover larger areas than clouds with positive or neutral buoyancy.

There are two fundamental breakup mechanisms by which liquid aerosols can be formed, mechanical and thermal.

Mechanical breakup forms aerosols by producing flows at speeds which result in surface stresses that cause liquid droplets of a given diameter to become unstable and breakup into smaller droplets. The maximum stable drop diameter can be related to the Weber number, N_{We}:

$$N_{We} = \frac{\rho_a u^2 d_d}{\sigma_d} \tag{1}$$

where, u, is the velocity of the liquid jet relative to ambient air. Experiments indicate that a critical Weber number value of 10 to 20 is sufficient to cause aerosolization for small orifice diameters [4] [5] [9].

Thermal breakup is encountered in releases of superheated liquids and is caused by the flashing of liquid to vapor and the subsequent bubble growth as well as the relative velocity between the vapor and liquid. Bubble growth proceeds in three stages (see [7], [27], [23], [17] and [4]):

1. A surface-tension controlled stage where the bubble grows from a critical radius, i.e., nucleation. The smallest bubble capable of growth has a radius of:

$$r_1 = \frac{2\sigma_d}{P_s - P_a} \tag{2}$$

2. An inertia-controlled stage where the bubble grows at a constant rate determined by the vapor pressure and the density of the superheated liquid. This process happens very fast (on the order of microseconds) and the final bubble radius is about 10 times that of r_0:

$$r_2 = 10 r_1 \tag{3}$$

3. An asymptotic stage where bubble growth is limited by heat transfer and follows a linear dependence on the square root of time:

$$r_3 = r_2 + \left[F \left(\frac{\rho_f}{\rho_0} \right) (\pi \alpha)^{1/2} \right] t^{1/2} \tag{4}$$

where, F is the flash fraction and α is the thermal diffusivity. The ratio of densities is a measure of the change in volume due to flashing. The last term is a measure of the rate of heat conduction from the liquid to the vapor. The factor multiplying the square root of time is referred to as the bubble growth rate and has the unit of $m/s^{1/2}$.

At small orifice diameters thermal breakup is mainly dominated by surface stresses due to relative velocity effects. The transition to full atomization is instantaneous and depends on a critical superheat value which yields a critical relative velocity value. At large orifice diameters the velocity effect diminishes and the flashing mechanisms leading to bubble growth dominates.

Bushnell and Gooderum [5] conducted experiments with water where atomization was induced by flowing water at ambient pressure into an evacuated chamber. They conducted experiments with orifice diameters ranging from 0.01 to 0.04 inches and reported a sudden transition to atomization. They correlated their results with superheat. For the experiments with 0.01 and 0.02 inch orifices,

$$\frac{(T_{sh} - T_s)}{T_{sh}} = 0.10 \tag{5}$$

and for 0.03 and 0.04 inch orifices:

$$\frac{(T_{sh} - T_s)}{T_{sh}} = 0.07 \tag{6}$$

Brown and York [4] conducted experiments with water and freon and reported that a critical superheat exists, beyond which the liquid atomized into fine droplets. The diameters considered by Brown and York varied from 0.02 to 0.08 inches.

Large scale experimental data pertinent to aerosolization and rainout are summarized in Tables 6, 7, 8, 9, 10, and 11. The data is reported by Lantzy [18], and the Center for Chemical Process Safety (CCPS) [11] [12]

It is apparent that at large orifice diameters the flashing process plays an important role in the aerosolization of the liquid droplets. Flashing is the conversion of internal energy stored in the liquid to available energy by which the liquid is vaporized. Therefore, it is reasonable to assume that the correlation of aerosolized liquid fraction for superheated liquid releases should correlate well with the total amount of available energy.

It is interesting to note that the transition region to flash atomization reported at small orifice diameters is much smaller than the transition regions reported by Lantzy [18] and subsequently by CCPS [11] [12] with 0.25 and 0.5 inch diameters.

Figure 2: Dependence of bubble growth rate on available energy

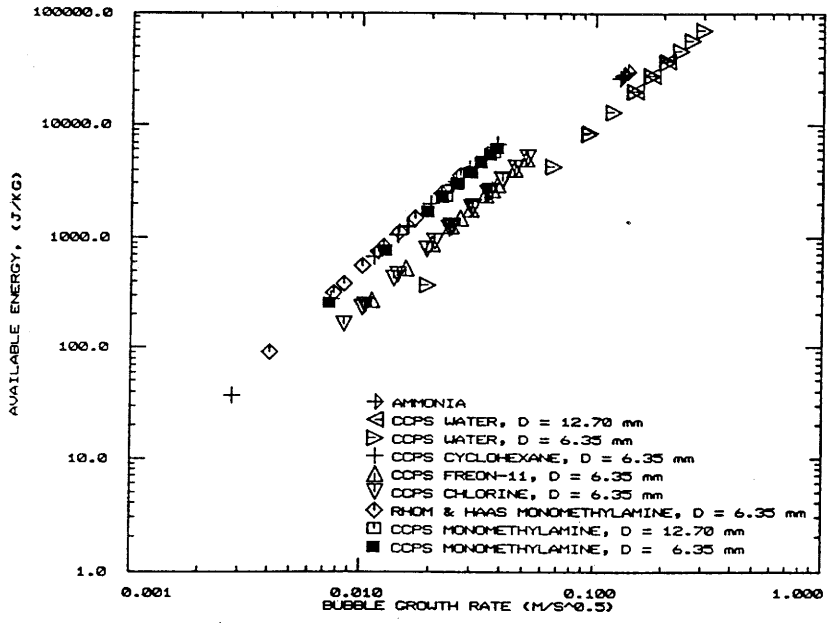

Figure 2 shows the calculated values of available energy for the data summarized in Tables 6, 7, 8, 9, 10, and 11 plotted against the bubble growth rate. It indicates that bubble growth is dominated by the amount of energy available in the liquid, A_E. A_E is the difference in internal energies between the initial and the final state minus the work done by expansion from the release pressure to ambient pressure.

We propose the following modification to the Weber number criteria for the calculation of a stable droplet diameter based on available energy:

$$N'_{We} = \frac{\rho_v A_E d_d}{\sigma_d} \tag{7}$$

Critical values for N'_{We} that reproduce the aerosol capture data reported by Lantzy and CCPS are on the order of 100. Typical model predictions for water and freon-11 capture data are shown in Tables 1 and 2. As noted earlier, predictions of liquid capture is very sensitive to droplet diameter. This becomes evident in the freon-11 data at droplet diameters lower than 400 micro-meters. Figure 3 shows a summary of calculated droplet diameters required to calculate a liquid capture equal to the experimental value.

Table 1: Model capture predictions for water, $N'_{We} = 100$

Release Diameter (mm)	Reported Capture	Calculated Capture	Calculated Droplet Diameter $\times 10^6$ (m)
6.350	0.86	0.865	1500
6.350	0.84	0.851	1302
6.350	0.83	0.850	1289
6.350	0.82	0.854	1341
6.350	0.80	0.851	1302
6.350	0.79	0.850	1289
6.350	0.77	0.833	837
6.350	0.76	0.801	548
6.350	0.74	0.788	559
6.350	0.73	0.783	553
6.350	0.70	0.784	551
6.350	0.69	0.760	407
6.350	0.64	0.636	309
6.350	0.62	0.339	304
6.350	0.62	0.681	399
6.350	0.61	0.549	306
6.350	0.61	0.333	309
6.350	0.59	0.406	241
6.350	0.54	0.388	195
6.350	0.47	0.235	159
12.75	0.72	0.787	549
12.75	0.69	0.674	403
12.75	0.65	0.510	303

Table 2: Model capture predictions for Freon 11, $N'_{We} = 200$

Release Diameter (mm)	Reported Capture	Calculated Capture	Calculated Droplet Diameter $\times 10^6$ (m)
6.350	0.620	0.813	1500
6.350	0.512	0.770	1269
6.350	0.514	0.646	764
6.350	0.475	0.472	536
6.350	0.323	0.261	455
6.350	0.306	0.02	373
6.350	0.108	0.00	282
6.350	0.038	0.00	225

Figure 3: Calculated droplet diameters at reported liquid capture data

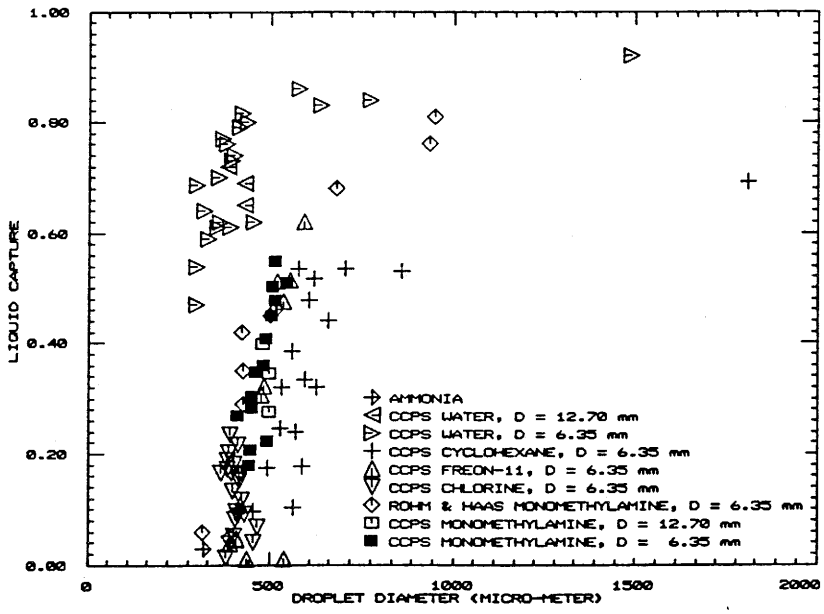

Rainout Criteria

The criteria used to determine whether a drop of a given size will rain out is based on hydrodynamic considerations. The drop is considered to remain airborne (no rain-out) if the rate at which the jet expands by entrainment exceeds its terminal settling velocity:

$$u_j \frac{dR}{ds} > u_t \tag{8}$$

The droplet terminal settling velocity is given by [26]:

$$u_t = \sqrt{g \frac{4}{3} \frac{\rho_{d_l}}{\rho_s} \frac{d_d}{C_D}} \tag{9}$$

where C_D is the drag coefficient and is given by the following expressions:

$$C_D = \frac{24}{N_{Re}} \quad , \mathrm{N_{Re}} < 0.1 \tag{10}$$

$$C_D = \frac{24}{N_{Re}} \left[1 + \frac{3}{16} N_{Re} + \frac{9}{160} N_{Re}^2 \ln(2N_{Re})\right] \quad , 0.1 \leq \mathrm{N_{Re}} < 2 \tag{11}$$

$$C_D = \frac{24}{N_{Re}} \left[1 + 0.15 N_{Re}^{0.687}\right] \quad , 2 \leq \mathrm{N_{Re}} < 500 \tag{12}$$

$$C_D = 0.44 \quad , 500 \leq \mathrm{N_{Re}} < 200{,}000 \tag{13}$$

N_{Re} is the droplet Reynolds number and is based on the relative velocity difference between the droplet and the surrounding medium:

$$N_{Re} = \frac{d_d |u_{d_s}| \rho_s}{\mu_s} \tag{14}$$

Droplet Evaporation

Droplet evaporation can be a significant factor in determining the fraction of rained-out liquid to reach the surface following an elevated continuous release of a superheated liquid. Droplet evaporation is significant for materials with low boiling points at ambient pressure. In this section a model based on conservation laws which predicts the temperature, trajectory, and mass evaporated for a single falling liquid droplet will be derived. This model is similar to the models developed by Papadourakis et al. [22], Vesala et al. [28], and Kukkonen et al. [14], [15], [16] and Woodward and Papadourakis [30].

Consider an evaporating spherical droplet moving in a gas medium where the evaporating mass is diffusing through the vapor phase. The change of droplet mass is a function of the mass transfer coefficient, the droplet surface area, and concentration difference:

$$\frac{dM_d}{dt} = -K_s A_d \left[C_d - C_s\right] \tag{15}$$

where A_d is the surface area of the droplet and is equal to:

$$A_d = \pi d_d^2 \tag{16}$$

Equation 15 is equivalent to:

$$\frac{dM_d}{dt} = -A_d K_s \rho_{d_s} \chi_1 \chi_2 \ln\left[\frac{1 - P_{d_s}/P_s}{1 - P_d/P_s}\right] \tag{17}$$

where ρ_{d_s} is the gas density of the droplet evaluated at ambient conditions, P_{d_s} is the partial pressure of the droplet material in the gas phase, and P_d is the saturation pressure at the droplet surface. If the drop is evaporating in pure air, then $P_{d_s} = 0$. The vapor density of the drop is calculated using the ideal gas law:

$$\rho_{d_s} = \frac{P_s M_{w_d}}{R_g T_s} \tag{18}$$

χ_1 and χ_2 are correction factors for the temperature effect on diffusivity for Stefan flow and for temperature dependence of the diffusion coefficients:

$$\chi_1 = 1 + \frac{P_d + P_{d_s}}{2P_s} \tag{19}$$

$$\chi_2 = \frac{T_s - T_d}{T_s^{\chi_3 - 1}} \frac{2 - \chi_3}{T_s^{2-\chi_3} - T_d^{2-\chi_3}} \tag{20}$$

$$\chi_3 = 1.8 \tag{21}$$

Stefan flow is defined as the additional mass flux leaving the surface of the droplet due to the relative motion of the center of mass of the air-vapor mixture to the droplet surface (See Wagner [29]).

The mass transfer coefficient can be calculated from empirical correlations relating the Sherwood number to the drop's Reynolds and Schmidt numbers:

$$K_s = \frac{D_{d_s} N_{Sh}}{d_d} \tag{22}$$

$$N_{Sh} = \alpha + \beta N_{Re}^{1/2} N_{Sc}^{1/3} \tag{23}$$

where α and β are constants having the values of 2 and 0.6 respectively [22, 28]. The Sherwood number is the ratio of total mass transfer to diffusive mass transfer. The Schmidt number is defined as the ratio of momentum to mass diffusivity:

$$N_{Sc} = \frac{\mu_s}{\rho_s D_{d_s}} \tag{24}$$

Assuming that no kinetic energy is converted into thermal energy, an overall heat balance for the droplet can be written as follows:

$$\frac{dM_d H_{d_l}}{dt} = A_d h\left(T_s - T_d\right) + \frac{dM_d}{dt} H_{d_v} + A_d \sigma \left[(1-r)T_s^4 - eT_d^4\right] \tag{25}$$

where σ is the Stephan-Boltzman constant which is equal to 5.6667×10^{-8} $\mathrm{J/m^2/s/K^4}$. The variables e and r represent the droplet surface emissivity and reflectivity. The first term on the right accounts for convective heat transfer, the second term accounts for evaporative cooling, and the last term accounts for radiative heat transfer.

Assuming constant heat capacities for the droplet material and using the same reference temperature for both vapor and liquid, the conservation of energy equation can be re-written as:

$$\begin{aligned} \frac{dT_d}{dt} &= \frac{1}{M_d C_{p_{d,l}}} \left[A_d h\left(T_s - T_d\right) + A_d \sigma \left((1-r)T_s^4 - eT_d^4\right)\right. \\ &+ \left.\frac{dM_d}{dt}\left[\Delta H_{d_{vl}} + \left(C_{p_{d,v}} - C_{p_{d,l}}\right)\left(T_d - T_0\right)\right]\right] \end{aligned} \tag{26}$$

where, the liquid and vapor enthalpies are given by:

$$H_{d_l} = C_{p_{d,l}}\left[T - T_0\right] + \lambda_{d_{vl}} \tag{27}$$

$$H_{d_v} = C_{p_{d,v}}\left[T - T_0\right] \tag{28}$$

In a similar fashion to mass transfer, the coefficient for heat transfer can be calculated from the Nusselt number which is defined as the ratio of total heat flux to conductive heat flux:

$$N_{Nu} = \frac{h d_d}{k_s} \tag{29}$$

The Nusselt number is calculated using the empirical relation:

$$N_{Nu} = \alpha + \beta N_{Re}^{1/2} N_{Pr}^{1/3} \tag{30}$$

where N_{Pr} is the Prandtl number and is defined as:

$$N_{Pr} = \frac{C_{p_s} \mu_s}{k_s M_w} \tag{31}$$

The droplet's momentum must be conserved in both the vertical and horizontal directions. The change of momentum in the horizontal direction is:

$$\frac{d(M_d u_{d,x})}{dt} = u_{d,x}\frac{dM_d}{dt} - C_D\frac{A_d}{4}\frac{1}{2}\rho_s u_{d,x} u_d \tag{32}$$

where u_d is defined by:

$$u_d = \sqrt{u_{d,x}^2 + u_{d,z}^2} \tag{33}$$

The first term of the right hand side of Equation 32 represents the momentum lost due to mass evaporated, and the second term represents momentum change because of the drag force.

Equation 32 is re-written to represent the change in the droplet horizontal velocity component:

$$\frac{du_{d,x}}{dt} = -\frac{1}{M_d}C_D\frac{A_d}{4}\frac{1}{2}\rho_s u_{d,x} u_d \tag{34}$$

The conservation of droplet momentum in the vertical direction is:

$$\frac{d(M_d u_{d,z})}{dt} = u_{d,z}\frac{dM_d}{dt} + gM_d\frac{\rho_s}{\rho_{d,l}} - gM_d - C_D\frac{A_d}{4}\frac{1}{2}\rho_s u_{d,z} u_d \tag{35}$$

The first term on the right hand side represents momentum lost due to mass evaporated, the second term represents the buoyancy force acting on the droplet, the third represents the droplet's weight, and the last term represents the vertical component of the drag force.

Equation 35 is re-written to represent the change in the droplet vertical velocity component:

$$\frac{du_{d,z}}{dt} = g\left(\frac{\rho_s}{\rho_{d,l}} - 1\right) - \frac{C_D}{M_d}\frac{A_d}{4}\frac{1}{2}\rho_s u_{d,z} u_d \tag{36}$$

Note the $u_{d,z}$ is positive if the droplet is moving upwards and negative if the droplet is falling.

The droplet position at any time is represented by the following trajectory equations:

$$\frac{dX_d}{dt} = u_{d,x} + U_w \tag{37}$$

$$\frac{dZ_d}{dt} = u_{d,z} \tag{38}$$

Figure 4: Rainout as a function of droplet diameter

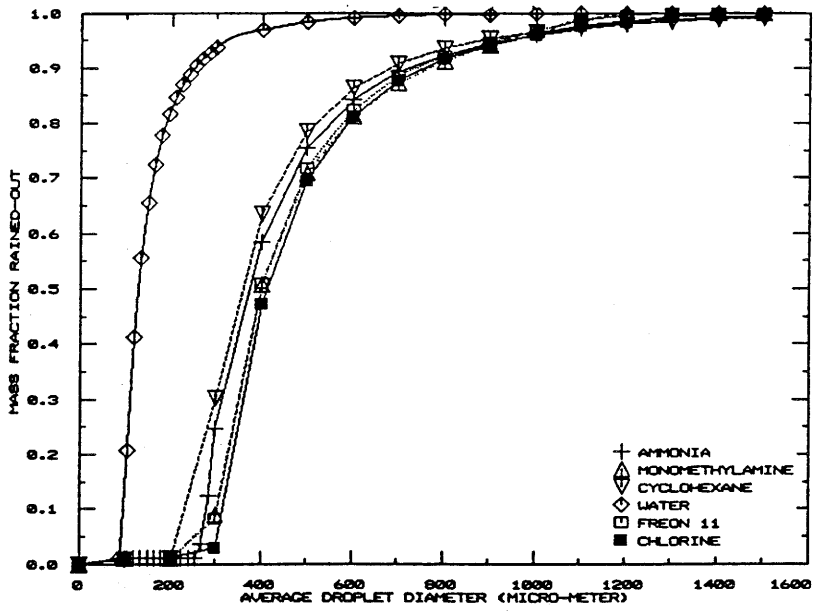

Figure 4 shows the effect of droplet diameter and boiling point on evaporation for ammonia, methylamine, cyclohexane, water, freon-11, and chlorine. The droplet evaporation was calculated by assuming a freely falling droplet at its boiling point using the following atmospheric conditions:

- Ambient temperature = 304 K
- Ambient pressure = 90000 Pa
- Release elevation = 1.22 m
- Wind speed = 5 m/s at 3 m elevation and a power law constant of 0.14

The graph illustrates the importance of droplet evaporation when droplet diameters are less than 400 microns. Under the same conditions, CCPS reported capture data that is consistent with the model predictions. For

chlorine the maximum liquid capture was about 20 % while for water it was about 87 %.

The slope of the curves shown in Figure 4 illustrate the sensitivity of droplet evaporation to increasing surface to volume ratio with decreasing droplet diameter. This indicates that an accurate estimate of droplet diameter is required to predict rainout for typical releases.

Two-Phase Flashing Jets

In references [20] and [21] one-dimensional conservation laws were derived by Ooms to describe the dispersion of gaseous jets. In this section we present a similar analysis for two-phase flashing jets with the following additions/modifications:

- Physical equilibrium is considered, and
- the velocity, density, and temperature profiles are assumed to be top-hat.

For simplicity, the jet conservation equations are presented for a three components system: air, water, and the dispersing chemical. The equations can be easily modified to handle more components.

Air entrained in the jet as it flows through the atmosphere is accounted for by the following three mechanisms (see [1],[10],[20] and [21]):

1. When the velocity of the jet is much larger than that of air, entrainment is assumed to be that of a free turbulent jet.
2. When velocity of the plume is approximately equal to that of air, entrainment is described as that of a cylindrical thermal plume in a stagnant atmosphere.
3. Turbulence of the atmosphere is also an important factor in calculating the amount of air entrained in the plume.

These three mechanisms are built into the following equation:

$$u_e = \alpha_1 \sqrt{\frac{\rho_m}{\rho_a}} |u - U_w \cos\theta| + \alpha_2 U_w \cos\theta |\sin\theta| + \alpha_3 u' \qquad (39)$$

where α_1 is the entrainment coefficient of a free jet (see [24]), α_2 is the entrainment coefficient for a line thermal, and α_3 is the entrainment coefficient caused by turbulence. The coefficients were assigned values of 0.057, 0.5 and 1.0 by Ooms [20][21].

The mixture density ρ_m is expressed as a function of the void fraction:

$$\rho_m = \alpha\rho_v + (1-\alpha)\rho_l \tag{40}$$

Free-jet type entrainment is caused by the parallel component to the jet centerline of the velocity difference between the jet and ambient air. The normal component causes generation of the vortex pair in the wake disturbing the jet boundary and producing strong mixing. This becomes important when the jet is bent over and is approximated by the term $\alpha_2 \cos\theta$ (see [1] and [20]).

The variable u' represents the root mean squared turbulent fluctuation velocity because of atmospheric turbulence. A typical value suggested by Ooms for u' is:

$$u' = (u_a^2)^{0.5} \tag{41}$$

where u_a is the wind velocity fluctuation. Briggs [3] [2] showed that:

$$u' = (\epsilon b)^{1/3} \tag{42}$$

where ϵ is the eddy energy dissipation. For a neutral atmosphere, Briggs assigns ϵ the value of $0.0677\frac{U_w}{y}$, for $y < 300$ m. For unstable atmosphere, Kaimal [13] assigns ϵ the value 0.004 and a value of 0 for stable atmosphere.

In the far field, entrainment is due solely to atmospheric turbulence. It can be estimated in a similar fashion to Gaussian models:

$$\alpha_3 u' = \frac{db}{ds} U_w \cos\theta \tag{43}$$

Assuming a circular cross sectional area proportional to the product $\sigma_y\sigma_z$, α_3 is equivalent to:

$$\alpha_3 = \frac{db}{ds} = \frac{b}{2}\frac{d}{ds}\ln(\sigma_y\sigma_z) \tag{44}$$

Typical values of the Gaussian standard deviations are reported as:

$$\sigma_y = ps^m \tag{45}$$

$$\sigma_z = qs^n \tag{46}$$

Then,

$$\alpha_3 = \frac{b}{2}\frac{m+n}{s} \tag{47}$$

Table 3: Dispersion Coefficients Parameters

Stability Class		p	m	q	n
very unstable	A	0.527	0.865	0.28	0.90
unstable	B	0.371	0.866	0.23	0.85
slightly stable	C	0.209	0.897	0.22	0.80
neutral	D	0.128	0.905	0.20	0.76
stable	E	0.098	0.902	0.15	0.73
very stable	F	0.065	0.902	0.12	0.67

Table 3 shows typical values of the parameters p, q, m and n for various atmospheric stability classes. Epstein et al. [6] used a similar approach to model jet growth in the far field due to atmospheric turbulence:

$$\alpha_3 u' = \frac{U_w}{2b}\frac{d}{ds}(\sigma_y \sigma_z) \tag{48}$$

The equations representing the characteristics of the jet are as follows:

Jet Z-coordinate

$$\frac{dZ}{ds} = \sin\theta \tag{49}$$

Jet X-coordinate

$$\frac{dX}{ds} = \cos\theta \tag{50}$$

Jet area

$$\frac{dA}{ds} - 2\pi b = 0 \tag{51}$$

Conservation of liquid mass

$$\frac{dm_T}{ds} - M_{w_w}\frac{dn_w}{ds} - M_{w_c}\frac{dn_c}{ds} = 0 \tag{52}$$

$$\frac{dn_T}{ds} - \frac{dn_w}{ds} - \frac{dn_c}{ds} = 0 \tag{53}$$

$$\frac{dm_T}{ds} - \frac{d}{ds}\rho_l u A(1-\alpha) = 0 \tag{54}$$

Conservation of vapor mass

$$\frac{dM_T}{ds} - M_{w_w}\frac{dN_w}{ds} - M_{w_c}\frac{dN_c}{ds} + M_{w_a}\frac{dN_a}{ds} = 0 \tag{55}$$

$$\frac{dN_T}{ds} - \frac{dN_w}{ds} - \frac{dN_c}{ds} - \frac{dN_a}{ds} = 0 \tag{56}$$

$$\frac{dM_T}{ds} - \frac{d}{ds}\rho_v u A \alpha = 0 \tag{57}$$

Individual species

$$\frac{dN_c}{ds} + \frac{dn_c}{ds} = 0 \tag{58}$$

$$\frac{dN_a}{ds} = \frac{2\pi b \rho_a u_e}{M_{w_a}} \frac{1}{1+\zeta} \tag{59}$$

$$\frac{dN_w}{ds} + \frac{dn_w}{ds} - \zeta\frac{dN_a}{ds} = 0 \tag{60}$$

where

$$\zeta = \frac{\frac{P_w}{P_a}\frac{\mathrm{RH}}{100}}{1 - \frac{P_w}{P_a}\frac{\mathrm{RH}}{100}} \tag{61}$$

Energy

$$H_a\frac{dN_a}{ds} + H_w\frac{dN_w}{ds} + H_c\frac{dN_c}{ds} + (H_w - \Delta H_{v,w})\frac{dn_w}{ds} + (H_c - \Delta H_{v,c})\frac{dn_c}{ds} + \left[N_a C_{p_a} + (N_c + n_c) C_{p_c} + (N_w + n_w) C_{p_w}\right]\frac{dT}{ds} - \left[H_a + H_w\zeta\right]\frac{dN_a}{ds} = 0 \tag{62}$$

Momentum in X-Direction

$$\frac{d}{ds}(M_T + m_T)\, u \cos\theta = C_D \pi b \rho_a U_w^2 |\sin^3\theta| + 2\pi b \rho_{a,w} U_w u_e \tag{63}$$

where, C_D is the drag coefficient with a default value of 0.3.

Momentum in Z-Direction

$$\frac{d}{ds}(M_T + m_T)\, u \sin\theta = Ag(\rho_a - \rho_m) - C_D \pi b \rho_a U_w^2 \cos\theta \sin\theta |\sin\theta| \tag{64}$$

Physical equilibrium

Assuming ideal behavior in both the liquid and vapor phase, the equilibrium constants for water and the dispersing chemical are obtained from their partial pressures:

$$K_w = \frac{P_w}{P_a} = \exp\left[A_w + B_w/T\right] \tag{65}$$

$$K_c = \frac{P_c}{P_a} = \exp\left[A_c + B_c/T\right] \tag{66}$$

The vapor pressure curve used in the equilibrium equations implies a constant heat of vaporization. It can be shown that the equations representing jet equilibrium are:

$$\frac{d}{ds}n_T N_c - K_c \frac{d}{ds}N_T n_c + \frac{n_c N_T K_c B_c}{T^2}\frac{dT}{ds} = 0 \tag{67}$$

$$\frac{d}{ds}n_T N_w - K_w \frac{d}{ds}N_T n_w + \frac{n_w N_T K_w B_w}{T^2}\frac{dT}{ds} = 0 \tag{68}$$

The equations representing physical equilibria are simple and will not predict the vapor-liquid equilibrium (VLE) behavior of highly non-ideal systems accurately. However, the near field impact of such predictions on jet temperature and jet vapor/liquid ratio is not significant because of the rapid entrainment of air.

For reactive materials such as hydrogen fluoride chemical equilibria must also be addressed. Simultaneous nonideal physical-chemical equilibrium can be calculated by direct minimization of the Gibbs free energy, as outlined by Saini [25]. Nonideal mixture behavior is represented by a modified Peng-Robinson equation of state [19].

Mathematically, the equilibrium problem is to minimize the total Gibbs free energy

$$G^t = \sum_{i=1}^{S} n_i \frac{G_i^\circ}{RT} + \sum_{i=1}^{N-S}\sum_{p=1}^{\pi} n_{ip}\left[\frac{G_i^\circ}{RT} + \ln\left(P\phi_{ip}\frac{n_{ip}}{n_{Tp}}\right)\right] \tag{69}$$

subject to the equality constraints,

$$C_1 \equiv \sum_{i=1}^{S} a_{ki} n_i + \sum_{i=1}^{N-S}\sum_{p=1}^{\pi} a_{ki} n_{ip} = b_k \qquad k = 1, \ldots, R \tag{70}$$

and the inequality constraints,

$$C_2 \equiv n_i \geq 0 \qquad i = 1, \ldots, S, \ldots, N\pi \tag{71}$$

where N the number of chemical species, π is the number of phases, S is the number of condensed solid species, n_{ip} is the equilibrium number of moles of the ith species in phase p, n_{Tp} is the total number of moles in phase p, G_i° is the standard Gibbs free energy of the i species evaluated at the system temperature T, P is the system pressure, a_{ki} is the number of atoms of element k in species i, b_k is the number of gram-atoms of element k, and R is the rank of the atom matrix (usually equal to the number of elements). The element abundance vector **b** is calculated as the product of the atom matrix **A** and the initial composition $\mathbf{n}^\circ$

$$\mathbf{An}^\circ = \mathbf{b} \tag{72}$$

The number of variables is equal to $((N-S)\times\pi+S)$, the number of equality constraints is equal to the rank of the atom matrix R, and the total number constraints is equal to the number of variables plus the number of equality constraints. The constrained Gibbs free energy minimization problem is solved efficiently using successive quadratic programming.

Equation of state

The ideal gas equation of state is used to represent the gas/vapor phase volumetric behavior:

$$\frac{d}{ds}\left[\rho_v T \frac{N_T}{M_T}\right] = 0 \tag{73}$$

A temperature dependent correlation is used to calculate saturated liquid densities:

$$\frac{d}{ds}\left[\frac{1}{\rho_l} - \frac{n_w v_w + n_c v_c}{m_T}\right] = 0 \tag{74}$$

where, v_w and v_c are the liquid molar volumes for water and the dispersing chemical. They are assumed to be a function of temperature only.

Ground Level Dispersion

Ground level dispersion is treated using the method of Epstein et al [6]. Epstein et al. modified the momentum equations to account for gravity compaction and sideward spreading. The ground level cross section is rectangular with a height of $2Z$ and a half-width of b. Entrainment is not allowed at jet-ground interface, so the perimeter of the jet is written as:

$$C = 4Z + \frac{A}{2Z} \tag{75}$$

At the transition to ground-jet dispersion, mass, concentration, and temperature are conserved. However, a discontinuity in b will exist at ground contact. A new variable, u_s, the jet spreading velocity, is added to the governing equations. The modified governing equations are:

Z-coordinate

$$\frac{dZ}{ds} = \frac{Z}{A}\frac{dA}{ds} - \frac{4Z^2}{A}\left[\frac{u_e + u_s}{u}\right] \tag{76}$$

X-coordinate

$$\frac{dX}{ds} = 1 \qquad \theta = 0 \tag{77}$$

Jet Area

$$A = 4Zb \tag{78}$$

Momentum for side edges

$$\frac{d}{ds}\left[u_s\left(m_T + M_T\right)\right] = 4gZ^2\left(\rho_m - \rho_a\right) \tag{79}$$

Momentum in axial direction

$$\frac{d}{ds}\left[\left(m_T + M_T\right)u\right] + g\frac{d}{ds}\left[\left(\rho_m - \rho_a\right)AZ\right] = U_w\rho_a u_e\left[4Z + 2b\right] \tag{80}$$

Model Validation

Validation of complex models, such as the one presented here, is a difficult task. Model validation should not be based solely on comparison with experimental data. For models incorporating a large number of parameters,

statistical evaluation would require a large number of experiments. Statistical evaluation based on limited experimental data can only *invalidate* a complex hazard model. Comprehensive model validation should focus on:

- correct representation of physical phenomena and underlying processes, i.e., **qualitative**,
- establishing first order derivatives, i.e, **sensitivity** analysis of model predictions to input parameters, and
- comparing predictions to measured values from experiments using a given **statistical** criterion.

The model described in this section was validated using large scale experimental data in both the near field and the far field. Near field validation was mainly concerned with air entrainment and its effect on temperature drop in value and location. Far field validation is mainly concerned with concentration profiles. Table 4 shows a range of predicted minimum temperature values for various chemicals. Figure 5 shows the concentration predictions for the Desert Tortoise ammonia experiments . Data summary is reproduced from Hanna et. al [8] and is described in Table 5.

Table 4: Minimum temperature predictions

Chemical	Reported (K)	Calculated (K)
Chlorine	203 - 205	203 - 210
Freon 11	253 - 273	245 - 257
Water	298 - 315	290 - 310
Cyclohexane	278 - 287	279 - 286
Methylamine	219 - 228	224 - 230

Table 5: Desert Tortoise Ammonia Experiments Data Summary (Reproduced from Hanna et al.)

Test Number	1	2	3	4
Date	8/24/83	8/29/83	9/1/83	9/6/83
Time	16:37 PDT	11:20 PDT	15:37 PDT	18:15 PDT
Release Conditions				
Exit Pressure (atm) (average)	10.00	11.02	11.23	11.64
Exit Temperature (K)	294.7	293.3	295.3	297.3
Nozzle Diameter (m)	0.081	0.0945	0.0945	0.0945
Spill Rate (kg/s)	79.7	111.5	130	96.7
Spill Duration (s)	126	255	166	381
Site Conditions				
Ambient Pressure (atm)	0.879	0.898	0.895	0.891
Relative humidity (%)	13.2	17.5	14.8	21.3
Air Temperature @ 2.5 m (K)	302.4	303.9	306.9	306.0
Soil Temperature (K)	304.8	303.8	304.8	304.0
Wind Speed @ 2 m (m/s)	7.4	5.8	7.4	4.5
(3 min average over 11 sites)				
σ_u (m/s)	1.2	0.7	1	–
σ_θ @ 2 m	5.7	7.5	8.3	5
Friction velocity (m/s)	0.44	0.34	0.45	0.27
Monin-Obukhov length (m)	93	95	571	45
Cloud cover (%)	1	4	70	1
Pasquill stability class	D	D	D	E
T(16 m) - T(2 m) (C)	0.87	0.46	0.13	0.9
Peak Concentrations (ppm)				
Averaging time (s)	80	160	120	300
100 m arc	50000	83200	76900	57300
800 m arc	8800	10800	7099	15400
Other arcs	328 (3500 m)	5000 (1400 m)	693 (1400 m)	3890 (2800 m)
	101 (5500 m)			

Figure 5: Far field model predictions

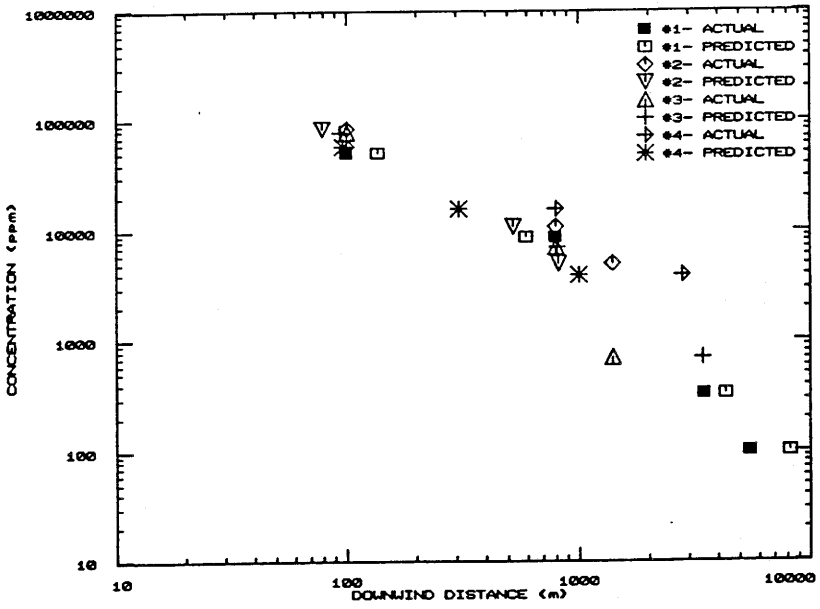

Table 6: CCPS Chlorine Data

T_0 K	P_0 kPa	D_0 mm	F_0	$\dot{M}$ kg/s	P_a kPa	T_a K	C %	T_{min} K	X_{min}	RH %	U_w m/s
247.4	147.2	6.35	0.035	0.31	90	303.3	23.4	204.6	1.52	8.6	6.8
256.4	257.0	6.35	0.064	0.49	90	303.6	21.5	204.9	1.52	8.9	7.7
250.9	215.5	6.35	0.046	0.44	90	301.2	20.2	205.2	1.52	10.6	6.0
247.1	178.9	6.35	0.034	0.38	90	304.3	18.9	206.1	1.52	23.6	5.8
261.8	303.3	6.35	0.080	0.55	90	300.7	18.1	202.5	3.04	14.1	6.0
251.5	225.9	6.35	0.048	0.44	90	303.8	17.1	204.6	1.52	8.9	4.9
258.1	258.5	6.35	0.069	0.48	90	304.6	16.6	205.4	1.52	23.4	5.3
272.8	362.2	6.35	0.115	0.51	90	304.3	16.6	205.4	1.52	10.9	10.8
245.4	183.7	6.35	0.028	0.39	90	300.5	16.5	206.3	1.52	11.9	6.1
267.4	358.6	6.35	0.098	0.60	90	303.5	16.2	204.0	3.04	14.0	9.9
272.4	420.8	6.35	0.114	0.64	90	302.9	15.2	203.4	3.04	8.0	7.2
267.6	295.9	6.35	0.099	0.45	90	303.9	13.2	204.6	1.52	11.7	8.8
261.3	586.0	6.35	0.079	0.81	90	300.9	11.7	202.2	1.52	10.8	6.4
273.3	433.9	6.35	0.117	0.65	90	304.3	9.6	206.3	1.52	22.0	4.9
267.1	639.1	6.35	0.097	0.84	90	303.8	9.2	203.4	3.04	15.0	7.6
277.9	482.3	6.35	0.131	0.70	90	304.8	9.0	204.6	1.52	15.1	6.1
278.1	417.5	6.35	0.132	0.54	90	305.3	8.1	205.4	1.52	14.3	6.1
261.8	922.5	6.35	0.080	1.05	90	300.5	6.8	202.5	3.04	10.7	6.9
283.7	558.9	6.35	0.149	0.74	90	305.8	5.3	204.9	1.52	15.3	7.1
267.1	979.1	6.35	0.097	1.07	90	303.3	4.1	203.1	3.04	13.4	10.0
283.6	567.2	6.35	0.149	0.76	90	303.5	3.9	203.7	1.52	7.2	7.5
289.2	661.1	6.35	0.167	0.83	90	303.3	1.3	205.4	1.52	26.4	5.2

Table 7: CCPS Freon 11 Data

T_0 K	P_0 kPa	D_0 mm	F_0	$\dot{M}$ kg/s	P_a kPa	T_a K	C %	T_{min} K	U_w m/s
308.95	163.5	6.35	0.0641	0.27	97	288.7	62.0	289.3	6.2
314.40	190.4	6.35	0.0906	0.32	97	289.3	51.2	253.7	6.7
319.94	224.1	6.35	0.1176	0.37	97	290.4	51.4	254.3	5.1
324.77	254.9	6.35	0.1412	0.40	97	288.7	47.5	251.5	5.1
327.32	269.7	6.35	0.1537	0.44	97	299.8	32.3	259.3	5.7
330.71	302.0	6.35	0.1706	0.46	97	294.0	30.6	273.2	3.3
336.13	343.9	6.35	0.1974	0.51	97	294.8	10.8	259.3	3.3
338.37	362.5	6.35	0.2083	0.53	97	301.5	4.7	273.2	5.1
338.42	366.7	6.35	0.2086	0.53	97	301.8	4.6	273.7	5.1
341.09	392.7	6.35	0.2220	0.54	97	295.9	3.8	262.0	1.8
348.81	470.6	6.35	0.2602	0.61	97	295.9	0.0	295.9	5.1
354.96	554.1	6.35	0.2912	0.67	97	298.2	0.0	298.2	4.6

Table 8: CCPS Water Data

T_0 K	P_0 kPa	D_0 mm	F_0	$\dot{M}$ kg/s	P_a kPa	T_a K	C %	T_{min} K	U_w m/s
378.4	202.6	6.35	0.012	0.348	97	300.4	92.0	329.8	4.9
398.7	253.1	6.35	0.050	0.354	97	295.7	86.0	315.3	4.1
410.8	347.6	6.35	0.073	0.372	97	308.2	84.0	304.8	4.1
411.0	344.4	6.35	0.073	0.380	97	308.7	83.0	304.8	5.7
410.2	346.8	6.35	0.072	0.420	97	300.1	81.7	302.0	3.6
410.8	343.2	6.35	0.073	0.405	97	308.2	80.0	304.8	6.2
411.0	347.2	6.35	0.074	0.403	97	308.7	79.0	303.7	5.1
421.0	460.4	6.35	0.093	0.488	97	300.9	77.0	300.3	4.1
433.2	632.9	6.35	0.116	0.568	97	297.9	76.0	300.9	6.4
432.6	616.5	6.35	0.115	0.527	97	304.8	74.0	302.6	
432.9	610.1	6.35	0.115	0.523	97	305.9	73.0	304.8	
433.0	610.9	6.35	0.116	0.539	97	305.9	70.0	304.2	
443.4	807.0	6.35	0.136	0.658	97	296.5	68.7	298.1	5.7
454.4	1062.3	6.35	0.157	0.797	97	299.3	64.0	301.4	3.6
455.3	1806.7	6.35	0.159	1.116	97	310.9	62.0	309.2	3.1
444.2	821.5	6.35	0.137	0.654	97	310.1	62.0	304.2	5.4
454.8	1031.4	6.35	0.158	0.746	97	305.9	61.0	307.0	2.8
454.4	1298.9	6.35	0.157	0.848	97	309.3	61.0	308.7	2.6
465.7	1361.0	6.35	0.180	0.901	97	300.1	59.0	300.9	4.1
476.4	1697.6	6.35	0.200	0.995	97	297.9	54.0	299.2	2.3
487.8	2109.0	6.35	0.224	1.144	97	303.2	47.0	304.8	4.1
433.1	631.1	12.75	0.116	2.408	97	303.2	72	307.6	2.6
443.8	816.1	12.75	0.137	2.750	97	308.7	69	310.3	3.9
455.3	1062.0	12.75	0.159	3.111	97	309.8	65	310.3	5.7

Table 9: CCPS Cyclohexane Data

T_0 K	P_0 kPa	D_0 mm	F_0	$\dot{M}$ kg/s	P_a kPa	T_a K	C %	T_{min} K	X_{min}	RH %	U_w m/s
369.1	156.0	6.35	0.112	0.222	90	309.9	69.2	286.8	1.52	9.3	5.5
365.2	217.4	6.35	0.088	0.300	90	308.8	53.5	279.4	3.04	13.3	3.1
353.7	182.9	6.35	0.020	0.260	90	308.4	53.4	283.1	3.04	12.8	5.2
359.9	209.1	6.35	0.057	0.283	90	309.2	51.7	280.1	3.04	17.4	3.2
381.3	213.3	6.35	0.189	0.288	90	307.4	53.0	281.9	3.04	22.7	4.3
370.7	192.6	6.35	0.122	0.272	90	309.8	47.6	279.9	3.04	9.3	7.1
376.1	256.0	6.35	0.155	0.331	90	309.1	44.1	279.4	3.04	12.2	2.9
370.9	239.5	6.35	0.123	0.315	90	308.7	38.4	278.9	3.04	17.5	4.2
382.1	282.9	6.35	0.194	0.357	90	308.8	33.4	279.9	3.04	20.5	4.5
387.4	309.9	6.35	0.228	0.375	90	309.1	32.1	278.9	3.04	12.2	3.1
381.3	251.2	6.35	0.189	0.326	90	309.4	31.9	279.9	3.04	8.2	7.0
392.5	274.0	6.35	0.261	0.346	90	309.9	24.7	279.4	3.04	8.2	5.4
392.9	318.2	6.35	0.263	0.378	90	310.0	23.9	278.1	3.04	6.2	3.8
392.8	354.7	6.35	0.263	0.406	90	309.6	17.6	278.1	3.04	7.2	3.1
382.9	556.0	6.35	0.199	0.533	90	310.5	17.5	279.6	3.04	13.2	3.6
398.2	383.7	6.35	0.299	0.414	90	310.1	10.3	278.1	3.04	12.2	4.0
398.4	391.9	6.35	0.300	0.428	90	308.0	9.5	277.9	3.04	8.2	2.2
343.3	140.1	6.35	0.000	0.199	90	309.8	70.6	285.1	1.52	6.2	3.5
348.3	140.8	6.35	0.000	0.203	90	310.5	69.3	283.6	1.52	8.2	5.7
337.6	142.1	6.35	0.000	0.211	90	309.2	71.0	285.3	1.52	9.2	3.7

List of Sym

A
A_E
b
D, d
C
C_D
C_p
F
g
G
h
H
k
K
L
m
M
Mw
n
N
N_{Pr}
N_{We}
N_{Ri}
N_{Re}
N_{Nu}
N_{Sc}
N_{Sh}
P
q
Q
R_g
RH
R, r
s
t
T
u
U
Uw
V
v
x
y
z

Table 10: CCPS Monomethylamine Data

T_0 K	P_0 kPa	D_0 mm	F_0	$\dot{M}$ kg/s	P_a kPa	T_a K	C %	T_{min} K	X_{min} m	RH %	U_w m/s
270.4	170.7	6.35	0.024	0.247	90	301.2	54.8	226.2	3.04	8.6	7.0
288.5	227.2	6.35	0.093	0.284	90	305.9	51.0	225.4	3.04	6.3	5.8
275.0	198.1	6.35	0.041	0.278	90	301.8	50.2	226.2	3.04	7.9	8.2
280.4	233.3	6.35	0.062	0.305	90	301.8	47.6	225.7	3.04	8.0	9.0
282.9	256.1	6.35	0.072	0.321	90	301.9	44.9	224.9	3.04	8.0	8.7
288.7	263.7	6.35	0.094	0.328	90	305.3	40.7	225.2	3.04	5.7	5.4
288.5	297.5	6.35	0.093	0.354	90	305.7	36.0	224.9	3.04	6.5	5.7
285.8	283.7	6.35	0.083	0.350	90	301.6	34.7	224.7	3.04	8.3	9.5
288.9	304.4	6.35	0.095	0.360	90	301.7	30.4	224.9	3.04	8.6	7.4
291.2	334.1	6.35	0.103	0.377	90	301.4	28.2	224.7	3.04	8.6	7.4
286.1	209.9	6.35	0.084	0.268	90	302.8	26.9	226.0	3.04	7.5	9.7
285.8	559.5	6.35	0.083	0.517	90	303.1	22.2	225.2	3.04	7.4	9.4
293.8	356.1	6.35	0.113	0.400	90	304.9	20.7	225.4	3.04	6.3	4.3
295.7	378.9	6.35	0.120	0.405	90	304.7	17.9	224.9	3.04	6.4	6.0
283.3	248.9	12.70	0.073	1.246	90	306.4	39.9	226.8	3.04	10.9	4.6
288.7	291.3	12.70	0.094	1.368	90	307.3	34.5	226.2	3.04	8.9	2.0
294.6	356.1	12.70	0.116	1.534	90	306.6	27.5	225.4	3.04	7.8	3.6

269	
276	
272	
274	
277	
273	
280	
278	
281	
281	

References

[1] G. Abraham. The flow of round buoyant jets issuing vertically into an ambient fluid flowing in a horizontal direction. In *5th International Water Pollution Research Conference*, page 15/1, 1970.

[2] G. A. Briggs. Plume rise. AEC Critical Review Series TID-25075, National Information Service, U.S. Department of Commerce, 1969.

[3] G. A. Briggs. Chimney plumes in neutral and stable surroundings. *Atmospheric Environment*, 6:507–510, 1972.

[4] R. Brown and J. L. York. Sprays formed by flashing liquid jets. *AIChE Journal*, 8(2):149–153, 1962.

[5] D. M. Bushnell and P. B. Gooderum. Atomization of superheated water jets at low ambient pressures. *Journal of Spacecraft*, 5(2):231–231, 1968.

[6] M. Epstein, H. K. Fauske, and G. M. Hauser. A model of the dilution of a forced two-phase chemical plume in a horizontal wind. In *1990 Spring National Meeting*, pages 1–40. AIChE, 1990.

[7] H. K. Forester and N. Zuber. Growth of a vapor bubble in a superheated liquid. *Journal of Applied Physics*, 25(4):474–478, 1954.

[8] S. R. Hanna, D. G. Strimaitis, and J. C. Chang. Evaluation of 14 hazardous gas models with ammonia and hydrogen fluoride field data. Technical paper, Sigma Research Corporation, 1991.

[9] J. O. Hinze. Fundamentals of the hydrodynamic mechanism of splitting in dispersion processes. *AIChE Journal*, 1(4):289–295, 1955.

[10] D. P. Hoult, J. A. Fay, and L. J. Forney. A theory of plume rise compared with field observations. *Journal of Air Pollution Control Association*, 19:585, 1969.

[11] Energy Analysts Inc. Release characteristics of superheated water and CFC-11 liquids. Experimental Data 90-05-540, The Center for Chemical Process Safety, 1990.

[12] Quest Consult
lamine, and cy
Chemical Proc

[13] J. C. Kaimal,
Turbulence st
33, 1976.

[14] J. Kukkonen
bulent two-ph

[15] J. Kukkonen
estimating th
association fo

[16] J. Kukkonen
borne droplet
19(7):871–87

[17] H. Kwak and
molecular int
1991.

[18] R. J. Lantzy
spheric relea
3:77, 1990.

[19] G. A. Melhe
equation of s

[20] G. Ooms. A
emitted by a

[21] G. Ooms, A
heavier thar
and Safety

[22] A. Papadou
bounds of d
Symposium,
Engineers,